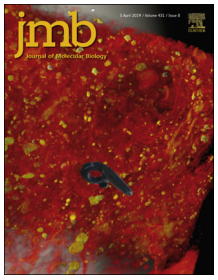

Cardiomyopathy Mutations in Metavinculin Disrupt Regulation of Vinculin-Induced F-Actin Assemblies

Muzaddid Sarker [1], Hyunna T. Lee [1], Lin Mei [2], Andrey Krokhotin [1], Santiago Espinosa de los Reyes [2], Laura Yen [3], Lindsey M. Costantini [4], Jack Griffith [4], Nikolay V. Dokholyan [1], Gregory M. Alushin [2] and Sharon L. Campbell [1]

*1 - **Department of Biochemistry and Biophysics and Lineberger Comprehensive Cancer Center,** University of North Carolina at Chapel Hill, Chapel Hill, NC 27599, USA*
*2 - **Laboratory of Structural Biophysics and Mechanobiology,** The Rockefeller University, New York, NY 10065, USA*
*3 - **Simons Electron Microscopy Center,** New York Structural Biology Center, New York, NY 10025, USA*
*4 - **Department of Microbiology and Immunology,** University of North Carolina at Chapel Hill, Chapel Hill, NC 27599, USA*

***Correspondence to Sharon L. Campbell:** campbesl@med.unc.edu.*
https://doi.org/10.1016/j.jmb.2019.02.024
Edited by: Prof. M.F. Summers

Abstract

Debilitating heart conditions, notably dilated and hypertrophic cardiomyopathies (CMs), are associated with point mutations in metavinculin, a larger isoform of the essential cytoskeletal protein vinculin. Metavinculin is co-expressed with vinculin at sub-stoichiometric ratios in cardiac tissues. CM mutations in the metavinculin tail domain (MVt) occur within the extra 68-residue insert that differentiates it from the vinculin tail domain (Vt). Vt binds actin filaments (F-actin) and promotes vinculin dimerization to bundle F-actin into thick fibers. While MVt binds to F-actin in a similar manner to Vt, MVt is incapable of F-actin bundling and inhibits Vt-mediated F-actin bundling. We performed F-actin co-sedimentation and negative-stain EM experiments to dissect the coordinated roles of metavinculin and vinculin in actin fiber assembly and the effects of three known metavinculin CM mutations. These CM mutants were found to weakly induce the formation of disordered F-actin assemblies. Notably, they fail to inhibit Vt-mediated F-actin bundling and instead promote formation of large assemblies embedded with linear bundles. Computational models of MVt bound to F-actin suggest that MVt undergoes a conformational change licensing the formation of a protruding sub-domain incorporating the insert, which sterically prevents dimerization and bundling of F-actin by Vt. Sub-domain formation is destabilized by CM mutations, disrupting this inhibitory mechanism. These findings provide new mechanistic insights into the ability of metavinculin to tune actin organization by vinculin and suggest that dysregulation of this process by CM mutants could underlie their malfunction in disease.

Introduction

Vinculin is an essential cytoskeletal protein that localizes to focal adhesions and adherens junctions [1,2]. At these sites of adhesion, vinculin acts as a scaffold to link transmembrane receptors to actin filaments, thereby playing a crucial role in cell adhesion, motility, and force transmission between cells and the cell–matrix interface. Without vinculin, defects in heart and nerve formation are observed, and mouse embryos do not survive past E10 [3]. In addition, lack of vinculin in cells leads to rounded morphology, increased motility [3,4] and resistance to apoptosis and anoikis [5].

Vinculin is a 117-kDa protein that functions as a molecular scaffold. It comprises a large 90-kDa head domain (Vh), a flexible proline-rich linker, and a 22-kDa tail domain (Vt) [6]. Vh interacts with talin at focal adhesions, α-catenin at cell–cell junctions, and α-actinin [7,8,9]. The proline-rich linker that connects Vh to Vt can bind to VASP, vinexin, CAP/ponsin, and the Arp2/3 complex [10,11,12,13]. Vt directly binds to filamentous actin (F-actin) [14], phosphatidylinositol 4,5-bisphosphate [15] and Raver1

[16]. Autoinhibitory interactions between Vh and Vt retain vinculin in its closed inactive state, which obscures ligand binding [6]. Although mechanisms of activation are not fully understood, it is currently believed that engagement of talin or catenin to Vh in conjunction with binding of additional ligands such as actin [2,7,17], post-translational modifications [18], and/or force [19,20,21,22] promotes activation and exposure of multiple ligand binding sites.

While vinculin is ubiquitously expressed, metavinculin, a larger splice isoform, is selectively expressed in smooth and cardiac muscle cells [23,24,25]. Metavinculin expression is tightly controlled at sub-stoichiometric levels relative to vinculin (9%–42%) and correlates with contractile needs of muscle cells [26,27]. Reduced metavinculin expression level is associated with cardiomyopathy (CM) and disorganized intercalated disc structures [28], suggesting that metavinculin is necessary for the maintenance of smooth muscle actin-membrane adhesion sites and in force generation and transmission through its interaction with the actin cytoskeleton.

While the tail domain of vinculin possesses an N-terminal strap (NtS) followed by a 5-helix bundle fold and a C-terminal hairpin (CtHP) [6], metavinculin contains an additional exon that encodes a 68-amino-acid insert between helix 1 (H1) and helix 2 (H2) within the tail domain (MVt) [23]. MVt also adopts a 5-helix bundle fold similar to Vt; however, the sequence that makes up H1 and NtS of Vt is displaced by homologous H1′ and NtS′ sequences contained within the 68-amino-acid insert [29]. Similar to vinculin, metavinculin can directly associate with F-actin [29,30,31]; however, unlike Vt, MVt does not bundle filamentous actin *in vitro* [30,31,32]. Point mutations identified within the 68-residue insert cause altered actin organization and heart disease, notably dilated cardiomyopathy (DCM) and hypertrophic cardiomyopathy (HCM) [28,32,33]. The A934V and ΔL954 metavinculin mutations are associated with DCM [32], whereas the R975W mutation has been identified in patients with both DCM and HCM [33]. Both DCM and HCM are diseases of myocardium that prevent normal blood flow within the heart resulting from disruption in force transmission, consistent with the prevailing notion that metavinculin–actin interactions play a key role in force transmission.

We and others have previously shown that binding of F-actin to Vt causes a conformational change in Vt that promotes dimerization and actin filament bundling [34,35]. However, the structure of the actin-induced Vt dimer is currently unknown. As H1 is sensitive to proteolysis upon addition of F-actin [36] and is not observed in our cryo-EM reconstruction of the Vt–actin complex [31], H1 likely partitions away from the helix bundle upon engagement with filamentous actin to promote vinculin dimerization. Similarly, electron density for metavinculin H1′ is lacking in the cryo-EM reconstruction of the metavinculin–actin complex [31]. Notably, the presence of displaced H1 appears to interfere with the ability of metavinculin to bundle F-actin, as its deletion promotes actin filament bundling [29].

While vinculin and metavinculin show similar modes of binding to F-actin, metavinculin is unable to bundle actin filaments. However, metavinculin mutants associated with DCM and HCM are able to form higher-order actin assemblies *in vitro* [32]. As metavinculin is co-expressed with vinculin in smooth muscle and cardiac tissues [23,25,26,27], it is likely that vinculin and metavinculin coordinately regulate the architecture of F-actin networks. In fact, we and others have previously observed that the presence of metavinculin at sub-stoichiometric ratios impairs vinculin-mediated F-actin bundling [31,36], suggesting that MVt may negatively regulate Vt-mediated actin bundling.

To better understand the coordinated role of metavinculin and vinculin in F-actin fiber assembly and the consequences of CM-related mutations, we conducted a series of actin co-sedimentation and negative-stain EM experiments utilizing MVt and Vt constructs. Consistent with our previous findings [31], MVt is unable to induce actin bundling, whereas the presence of sub-stoichiometric amounts MVt relative to Vt inhibits the assembly of actin filaments into parallel bundles. In contrast to wild-type (WT) MVt, and consistent with previous fluorescence microscopy data [32], MVt CM mutants alone weakly induce the formation of disordered higher-order F-actin assemblies. Strikingly, in the more physiological scenario of Vt–MVt mixtures, CM mutants lose the ability to inhibit Vt-mediated bundles, instead promote the formation of very large assemblies, which are morphologically consistent with aggregations of Vt-mediated bundles. To investigate the molecular basis for MVt's negative regulation of Vt-mediated actin bundling, we performed discrete molecular dynamics (DMD) simulations. Actin binding to vinculin promotes release of H1 from the tail domain helix bundle, exposing an interface in vinculin that promotes dimerization [31]. However, in the case of metavinculin, our simulations suggest that the insert and displaced H1 form a new structural element, a protruding sub-domain, with H1′ released from the helix bundle upon actin binding. This additional MVt sub-domain, generated upon actin engagement, could sterically block actin assembly into parallel F-actin bundles. Our DMD simulations also indicate that CM mutations within the C-terminus of metavinculin destabilize formation of this protruding actin-induced sub-domain, likely exposing residues which can mediate the formation of disordered assemblies. In summary, our results provide new mechanistic insights into the coordinated activities of vinculin and metavinculin in controlling F-actin network architecture and suggest that

regulation of vinculin-mediated actin bundling activity by metavinculin constitutes one key function that is compromised by the CM mutants.

Results

WT MVt domain does not induce F-actin bundling

The F-actin binding sites of vinculin and metavinculin are located in their tail domains, Vt and MVt, respectively, but these binding sites are occluded in the context of the full-length proteins due to autoinhibitory interactions between the head and tail domains. As the tail domains are functional in isolation, we have used recombinantly expressed Vt and MVt protein constructs in this study (shown by schematics in Fig. 1A) to probe the effects of MVt WT and MVt CM mutations on the formation of actin assemblies in the absence and presence of Vt. The Vt domain encompasses 188 C-terminal residues of vinculin and consists of five α-helices (H1–H5) flanked on both sides by flexible regions, an NtS and a CtHP. MVt contains an extra 68-residue insert between helices H1 and H2 of the corresponding sequence of Vt. Part of the insert displaces the 37 N-terminal residues comprising H1 (PDB ID 3MYI) and the NtS, with H1′ and NtS′ [29]. Here we investigate single-point mutations specific to the metavinculin insert region, namely, A934V, ΔL954 and R975W, associated with CMs and atherosclerosis [32,37]. We have also utilized a construct we designate as MVtp, which includes the additional 21-residue proline-rich linker preceding the NtS of MVt.

The core regions of both Vt and MVt comprise a compactly folded H2–H5 bundle. In the absence of actin, the H1–H5 helices are observable in X-ray crystal structures of full-length vinculin and Vt, and correspondingly, H1′–H5 are resolved in crystal structures of full-length metavinculin and MVt [29]. However, the regions preceding the H2–H5 bundle in both Vt and MVt were not detectable in our previously published cryo-EM reconstructions of these domains bound to F-actin [31]. We reported a twisting structural rearrangement of H2–H5 concomitant with actin binding that displaces H1/H1′ from the helical bundle by remodeling its hydrophobic core, which we inferred renders these regions disordered and/or dynamic. Vt and MVt both engage F-actin in an indistinguishable manner at subnanometer resolution through their compactly folded H2–H5 regions [31], which are identical in sequence (Fig. 1B).

Before investigating the effects of CM mutants, we first validated our WT Vt and MVt constructs to recapitulate previously reported binding and bundling activities [30,31,32,36], and also verified F-actin bundling inhibition by both MVt and MVtp proteins. We acquired negative-stain EM images of actin filaments in the absence and presence of WT

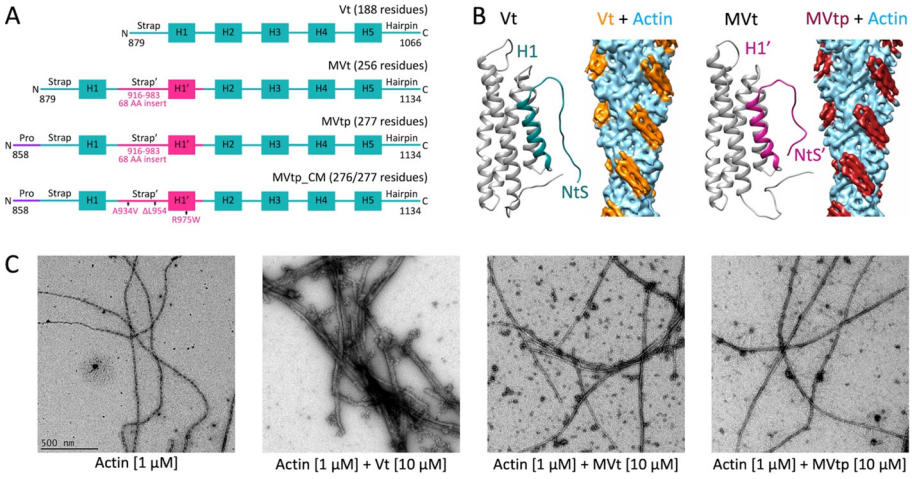

Fig. 1. MVt domain exhibits similar F-actin binding affinity but dramatically reduced bundling (crosslinking) of the filaments relative to the Vt domain. (A) Schematic representation of Vt and MVt constructs used in this study. Vt consists of five α-helices (H1–H5) flanked by an NtS and a CtHP. MVt contains a 68-residue insert between helices H1 and H2 that replaces the original H1 and NtS by H1′ and NtS′. MVtp includes the 21-residue proline-rich linker preceding the NtS of MVt. Mutations within the metavinculin insert region, namely, A934V, ΔL954 and R975W, have been identified in CMs. (B) X-ray crystal structures of Vt (PDB ID 1TR2) and MVt (PDB ID 3MYI) as well as the cryo-EM reconstruction of Vt–actin (EMD-6446) and MVt–actin (EMD-6447) interfaces. Vt and MVt comprise a highly similar 5-helix bundle fold in the absence of actin, where H1′ of MVt swaps with H1 of Vt. Upon actin engagement, regions N-terminal of H2 are not detectable in the cryo-EM reconstructions. (C) Negative-stain EM images of actin filaments. Micrographs are acquired at the same magnification (scale bar represents 500 nm, shown in the left panel). Crosslinking or bundling of actin filaments by Vt generates thick fibers. In contrast, MVt and MVtp do not promote actin filament bundling.

Vt, MVt and MVtp (Fig. 1C). The actin-alone sample showed single, linear actin filaments, whereas Vt induced crosslinking of filaments into parallel bundles as expected, resulting in the formation of thick fibers. When either MVt or MVtp was added to F-actin instead of Vt, F-actin bundling was dramatically reduced, with few observable thick fibers. This is consistent with previous reports by our group and others that MVt does not induce large linear actin bundles like Vt [30,31,32,36], indicating that the MVt insert region prohibits actin-induced MVt dimerization and negatively regulates F-actin bundling. In addition, inclusion of the proline-rich linker, as in MVtp, has a minor, albeit significant effect on its regulatory activity.

MVt CM mutants induce higher-order F-actin assemblies

Having validated our constructs and confirmed similar behavior of MVt and MVtp by negative-stain EM (Fig. 1C), we next used F-actin co-sedimentation assays to examine the F-actin binding and aggregation activities of MVtp constructs featuring the CM mutations A934V, ΔL954 and R975W. First, we compared the F-actin binding of MVtp WT and CM mutants relative to Vt. Samples containing actin (10 or 20 μM) plus individual tail domains (10 μM) were subjected to high-speed centrifugation (see Materials and Methods for experimental details). Under these conditions, the supernatant (S) contains unbound tail domain, while the pellet (P) contains F-actin and bound protein. The amount of tail domain present in each fraction was analyzed by SDS-PAGE (Fig. 2A) and quantified using ImageJ [38]. WT Vt, MVt, and MVtp, as well as all three MVtp CM mutants, exhibited similar binding affinity to F-actin (Fig. 2B). From these data, we conclude that MVt mutations do not impair F-actin binding. This is consistent with the known actin binding interface, comprising the compactly folded H2–H5 region,

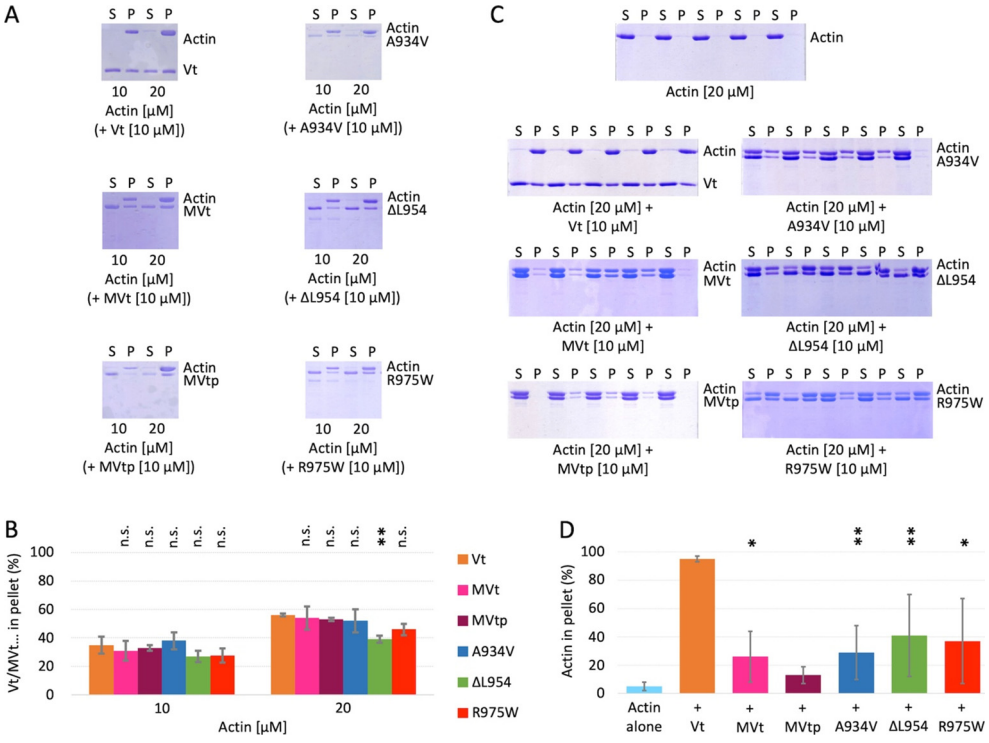

Fig. 2. MVt domain WT and CM mutants exhibit similar F-actin binding but differ in the ability to form higher-order actin assemblies. (A) Representative SDS-PAGE results obtained from high speed F-actin co-sedimentation (100,000 g, 30 min) assays in the presence of Vt, MVt, or MVtp WT and CM proteins (S, supernatant; P, pellet). (B) Quantification of protein fractions present in pellets representing individual sub-populations of Vt, MVt, or MVtp constructs bound to F-actin. Error bars represent standard deviation (SD) (n = 2, 2 replicates for each n). (C) Representative SDS-PAGE results obtained from low-speed F-actin co-sedimentation (12,000 g, 15 min) assays in the presence of Vt, MVt, or MVtp WT and CM proteins. (D) Quantification of actin fractions in pellets representing sub-populations of F-actin present in bundles or in higher-order assemblies induced by Vt, MVt, or MVtp constructs. Error bars represent SD (n = 2, 5 replicates for each n). Vt and MVt or MVtp WT (labeled as MVt and MVtp), as well as all MVtp CM mutants (labeled as A934V, ΔL954 and R975W), bind actin filaments similarly. However, while Vt drives almost the entire population of actin filaments into bundles or higher-order assemblies (~95%), MVt or MVtp WT display little assembly formation (~15%–20%). In contrast, increased F-actin assembly formation is observed for MVtp CM mutants (~30%–40%) compared to MVtp WT. Statistical significances in panels B (with respect to Vt) and D (with respect to MVtp) are indicated by the following: non-significant (n.s.), $*p < 0.05$, $**p < 0.01$.

which is not predicted to be impacted by any of the CM mutations [31].

We next employed low-speed centrifugation assays to assess the F-actin crosslinking activities of this same panel of constructs (see Materials and Methods for experimental details). Under these conditions, only large cross-linked assemblies of F-actin and bound protein are pelleted, while individual actin filaments are retained in the supernatant. The fraction of actin present in the pellet was quantified as described above to determine the subpopulations of F-actin involved in higher-order assemblies (Fig. 2D). It should be noted that while this is often referred to as a "bundling" assay, the pellets from low-speed centrifugation may contain both thick fibers representing canonically bundled actin filaments, as in the case with Vt (Fig. 1C), but also other sufficiently large structures (ordered or disordered) that pellet under these conditions. These assays were conducted in parallel with negative-stain EM, to visualize the actin assemblies formed in the presence of Vt and MVt proteins. For isolated F-actin, little actin was found in the pellet (~5%), but upon the addition of Vt, almost all of the F-actin was found in the pellet (~95%), consistent with the negative-stain EM data (Fig. 1C). Also consistent with the negative-stain EM results (Fig. 1C), the amount of actin found in the pellet was dramatically reduced when MVt was added (~26%) and to an even lower amount when MVtp was added (~13%). Interestingly, an increase in the amounts of pelleted actin was found for the MVtp CM mutants: A934V (~29%), ΔL954 (~41%), and R975W (37%).

Quantitative negative-stain EM assay probes F-actin assemblies

To visualize and quantify differences in actin filament organization in the presence of Vt and MVt WT, as well as MVt CM mutants, we developed a quantitative negative-stain transmission electron microscopy (TEM) assay (Fig. 3, Supplementary Fig. 1). The quantitative power of traditional negative-stain EM imaging of F-actin assemblies is limited by selection bias, as choosing which part of the grid to image is dependent on input of an experienced user. In addition, the frequently irregular structure of these assemblies, compounded by their inherently variable contrast after negative staining, is refractory to image analysis methodology which depends on classification or averaging.

To overcome selection bias, we targeted grid squares at low magnification where their contents were invisible. We then imaged the entirety of each targeted square at a magnification sufficient to resolve individual actin filaments, tiling it with overlapping fields of view which were subsequently stitched together (Fig. 3A). We next implemented an image analysis procedure to detect and quantify the size of higher-order assemblies which is insensitive to their variable internal structure. Images were thresholded (the only step requiring user input due to stain variability) and binarized, then automatically segmented into continuous regions using the "Analyze Particles" procedure in ImageJ [38]. To analyze these data, we plot the cumulative fraction of F-actin + bound proteins detected in all regions *versus* region size (Fig. 3C, Supplementary Fig. 1), which we find to be a sensitive metric of higher-order assembly state that is robust against variations in background noise between different datasets (see Materials and Methods for details).

MVt CM mutants form mesh-like actin assemblies

To validate this assay, we first examined the known differential F-actin assembly properties of Vt, which strongly bundles actin, in comparison to MVt WT, which does not induce assemblies as previously established [30,31,32,36], and here re-validated through qualitative negative-stain EM and quantitative low-speed co-sedimentation assays (Figs. 1C and Fig. 2C–D). As expected, although other assembly states are present as a minor fraction, we find that the presence of Vt primarily induces the formation of linear actin bundles (Fig. 3A) and correspondingly shifts the distribution towards larger assemblies *versus* actin alone (Fig. 3C). While the presence of MVt WT did produce a slight but significant shift relative to actin alone, the effects were modest, with substantially fewer large assemblies than for Vt (Fig. 3C). Consistently, no obvious bundles and few other assemblies were visible in the images, which were qualitatively similar in appearance to F-actin alone (Fig. 3A).

We next examined the effects of MVt CM mutants. These experiments, which require small amounts of material, were initiated mostly with the tail domain constructs (i.e., MVt) and later we confirmed that inclusion of the proline-rich linker (i.e., MVtp) does not adversely affect metavinculin's regulatory role (Figs. 1C and 2C–D). Thus, we investigated R975W and ΔL954 in the MVt background and MVtp A934V in our negative-stain EM experiments. As our studies establish MVt and MVtp show similar activity profiles (Figs. 1 and 2), we believe that experiments between mutants in these backgrounds can safely be compared.

Consistent with low-speed co-sedimentation assays (Fig. 2C–D), we observed a significant increase in assemblies in the presence of CM mutants MVtp A934V, MVt ΔL954, and MVt R975W, with R975W having the most dramatic effect (Fig. 3C), in accordance with the severity of disease caused by this mutation in patients [32,33]. Examination of the images shows primarily an irregular, mesh-like organization of actin filaments (Fig. 3B), unlike the majority species present as linear bundles formed in the presence of Vt (Figs. 1C and 3A).

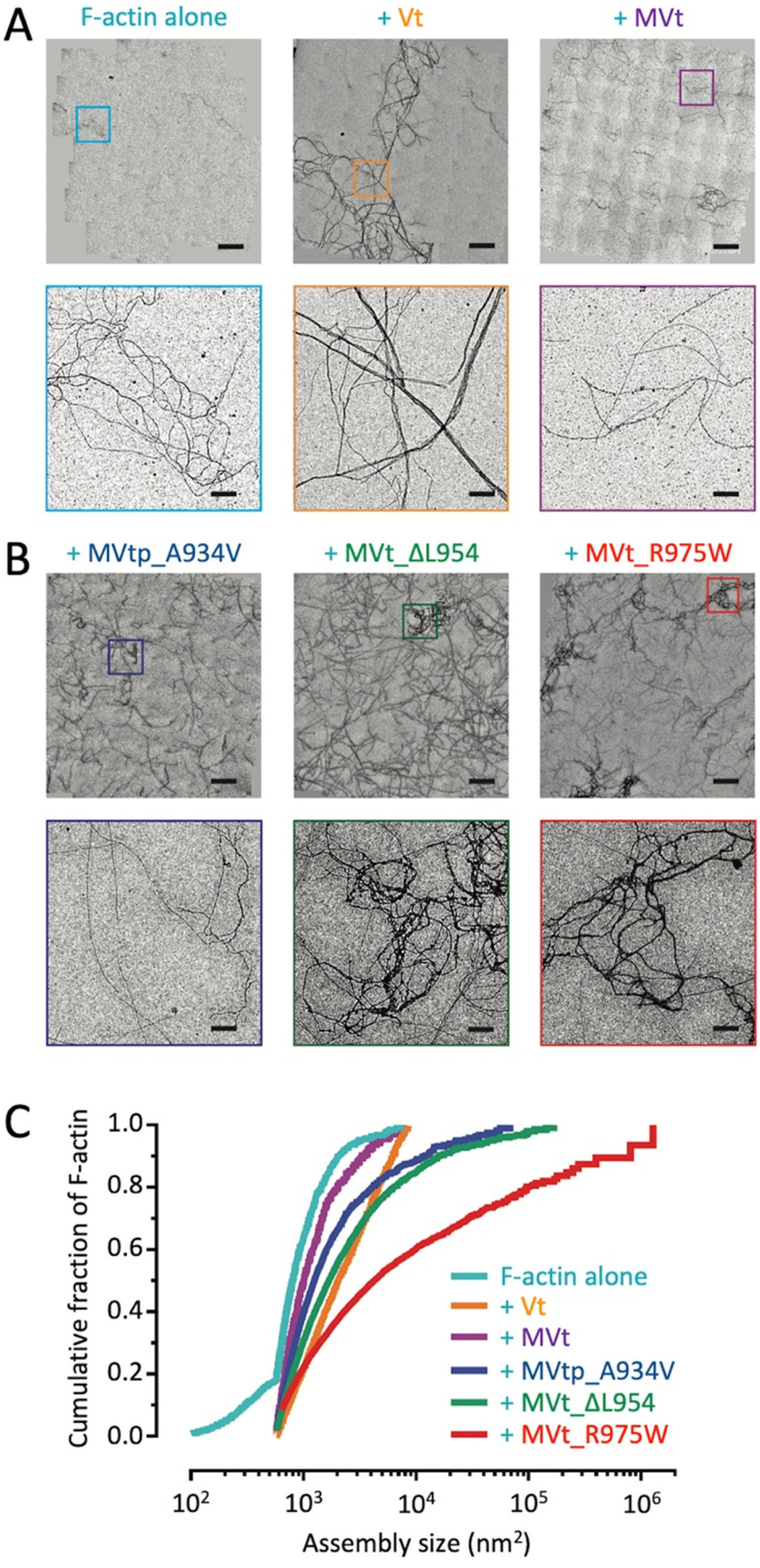

Fig. 3. Metavinculin CM mutants promote formation of disordered, mesh-like F-actin assemblies. (A) Stitched negative-stain EM images of F-actin alone and in the presence of WT Vt and MVt proteins (bars represent 10 μm). Zoomed views of the boxed regions are shown in the bottom panel (bars represent 1 μm). (B) Stitched negative-stain EM images of F-actin in the presence of MVt or MVtp proteins featuring CM mutations (bars represent 10 μm). Zoomed views of the boxed regions are shown in the bottom panel (bars represent 1 μm). (C) Cumulative plots of F-actin assemblies from the indicated conditions. Pairwise comparisons show all distributions to be significantly different (KS test, $p < 0.01$). $N \geq 10$ fields and $n \geq 764$ regions were quantified for each condition. F-actin, 0.5 μM; Vt/MVt/MVtp constructs, 2.0 μM.

MVt CM mutants fail to inhibit Vt-induced higher-order actin assemblies

Metavinculin is co-expressed with vinculin at sub-stoichiometric levels in smooth muscle and cardiac tissues [25,26,27]. We and others have previously reported that the presence of sub-stoichiometric MVt impairs Vt-mediated F-actin bundling [31,36]. Hence, metavinculin likely acts as a negative regulator of vinculin-mediated F-actin bundling. Here, we employed low-speed pelleting assays to probe the effects of MVtp CM mutants in comparison to MVtp WT, on Vt-induced F-actin assemblies. Three sets of actin co-sedimentation data were acquired, with 20 μM actin and Vt:MVtp at 5:5, 10:10, and 10:5 μM (Fig. 4). Supernatant and pellet fractions were analyzed by SDS-PAGE (Fig. 4A–C) and quantified (Fig. 4D) as described above. In the presence of MVtp WT, a proportionate reduction of Vt-induced F-actin assemblies was observed: as ~47–52% F-actin was found in the pellet for Vt:MVtp at 1:1 and ~74% F-actin was found in the pellet for Vt:MVtp at 2:1, as opposed to 95% F-actin in the pellet for Vt alone. Interestingly, for all 3 MVtp CM mutants, at both 1:1 and 1:2 ratios with Vt, almost all of F-actin was found in the pellet fractions: ~87–95% for A934V, ~81–90% for ΔL954, and ~84–89% for R975W. Thus, in a dramatic contrast to the MVtp

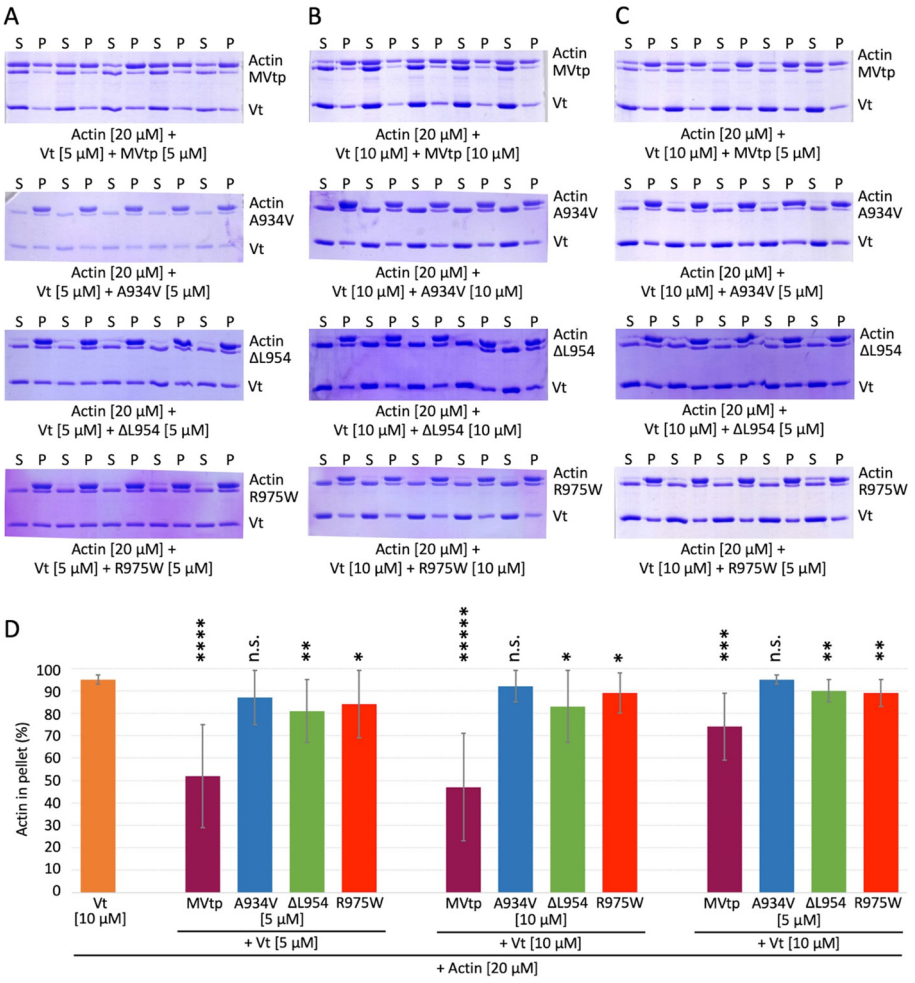

Fig. 4. MVt CM mutants fail to inhibit Vt-induced F-actin bundling. (A–C) Representative SDS-PAGE analysis of low-speed F-actin co-sedimentation (12,000 g, 15 min) assays incubated with Vt in the presence of MVtp WT protein (labeled as MVtp) or MVtp CM mutants (labeled as A934V, ΔL954, and R975W) at indicated concentrations (S, supernatant; P, pellet). (D) Quantification of the actin fraction present in pellets representing higher-order F-actin assemblies that include F-actin bundles in case of Vt. Error bars represent standard deviation (SD) (n = 2, 5 replicates for each n). At both 1:1 and 2:1 ratios with Vt, MVtp WT proportionately reduces the amounts of higher-order F-actin assemblies, but in all cases, MVtp CM mutants fail to inhibit such Vt-induced higher-order F-actin assemblies. Statistical significances in panel D are indicated by the following: non-significant (n.s.), *$p < 0.05$, **$p < 0.01$, ***$p < 0.001$, ****$p < 0.0001$, *****$p < 0.00001$ with respect to Vt.

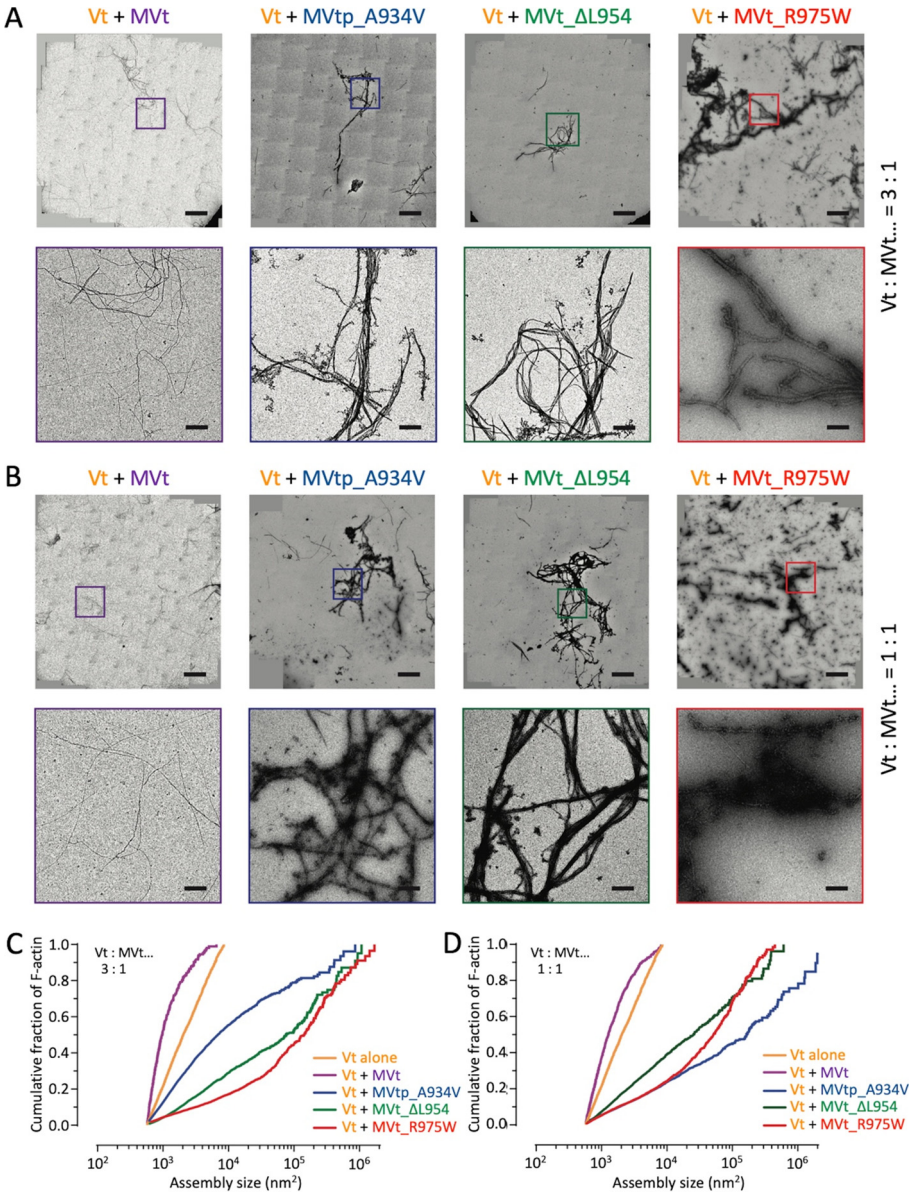

Fig. 5. MVt CM mutants aggregate Vt-induced actin bundles. (A) Stitched negative-stain EM images of F-actin in the presence of Vt + WT or CM mutant MVt(p) at Vt to MVt(p) ratio of 3:1 (bars represent 10 μm). Zoomed views of the boxed regions are shown in the bottom panel (bars represent 1 μm). F-actin 0.5 μM, Vt 3.75 μM, and MVt(p) 1.25 μM. (B) Stitched negative-stain EM images of F-actin in the presence of Vt + WT or CM mutant MVt(p) at Vt to MVt(p) ratio of 1:1 (bars represent 10 μm). Zoomed views of the boxed regions are shown in the bottom panel (bars represent 1 μm). F-actin 0.5 μM, Vt 2.5 μM, and MVt(p) 2.5 μM. (C) Cumulative plots of F-actin assemblies in the presence of Vt to MVt(p) at ratio of 3:1. (D) Cumulative plots of F-actin assemblies in the presence of Vt to MVt(p) at ratio of 1:1. Pairwise comparisons show all distributions to be significantly different (KS test, $p < 0.0001$) in panels C and D. N > 10 fields and n > 655 regions were quantified for each condition in panel C, and N > 10 fields and n > 2241 regions were quantified for each condition in panel D. Vt alone data are replotted from Fig. 3.

WT, the amount of F-actin existing in the pellets representing higher-order actin assemblies was reduced only marginally by the MVtp CM mutants. These results indicate that unlike WT MVt or MVtp, MVtp CM mutants are unable to negatively regulate higher-order actin assemblies in the presence of Vt.

MVt CM mutants coalesce Vt-mediated bundles into large higher-order actin assemblies

We next employed negative-stain EM to visualize the morphology and quantify the size distributions of higher-order assemblies formed in the presence of

both Vt and MVt or MVtp WT and CM mutants. Consistent with previous reports [30,32,36] and co-sedimentation assays (Fig. 4), we find that the presence of MVt WT inhibits the bundling activity of Vt at both a sub-stoichiometric 1:3 ratio (Fig. 5A, C) and a stoichiometric 1:1 ratio (Fig. 5B, D). An examination of the images suggests a reduction in large parallel bundles (Fig. 5A, B). However, we find that all MVt or MVtp CM mutants dramatically increase the size of F-actin assemblies formed in the presence of Vt, at both ratios (Fig. 5A–D). These results are consistent with our co-sedimentation assays demonstrating almost the entire population of actin pelleting in the presence of Vt + MVtp CM mutants as with Vt alone (Fig. 4), but additionally suggest that even larger assemblies are formed than in the presence of Vt alone.

The morphology of these assemblies is consistent with a combined effect between what we observe for the MVt or MVtp CM mutants alone, which primarily form disordered meshes (Fig. 3B) and Vt-mediated bundling. Linear bundles are clearly visible (Fig. 5A–B); however, these are frequently coated with large, amorphous aggregates (Fig. 5A–B), which are rarely observed in the presence of Vt alone, MVt alone, or Vt + MVt WT (Fig. 3A–B). This observation is consistent with MVt or MVtp CM mutants driving the coalescence and aggregation of Vt-induced actin bundles rather than inhibiting their formation, as is the case for MVt WT.

The MVt-specific insert region forms an additional sub-domain upon actin binding

In the cryo-EM reconstruction of the MVt–F-actin complex [31], density for the N-terminus, including H1′, the displaced H1, and straps, was not observable. This is likely due to dynamics or disorder associated with these regions. To gain structural insight into rearrangements associated with MVt NT, CT, and the insert upon actin binding, we employed DMD simulations [39]. Our model system comprises a single MVt including residues 896–1134 bound to an actin homodimer (F-actin) using the deposited model based on the cryo-EM reconstruction as the starting point (PDB ID 3JBK) for MVt residues 985–1115 and actin. The simulations were performed using replica exchange for 2 million steps (see Materials and Methods for details). One hundred minimal energy structures were selected and clustered.

We identified two clusters (Fig. 6), which differ in N- and C-termini conformations. While structures from the first cluster have tightly intertwined N- and C-termini (Fig. 6A), structures from the second cluster show the C-terminus interacting with the surface of F-actin (Fig. 6B). The common feature of both clusters is formation of a new additional structural sub-domain protruding outwards from F-actin. We further explored stability of the protruding sub-domains in both clusters. We subjected structures representing centroids of these clusters to DMD simulations. For each structure, we ran 10 independent simulations at two different temperatures [T_1 = 0.5 kcal/(mol k_B) and T_2 = 0.55 kcal/(mol k_B)]. In further support of the protruding MVt sub-domain that is formed upon F-actin engagement, the insert-dependent protruding structural element did not unfold and appeared stable throughout the simulations (Supplemental Videos 1 and 2). We argue that this sub-domain mediates unique biological functions of MVt relative to Vt, such as the inability to produce F-actin bundles [30,31,32] and the ability to suppress Vt-mediated F-actin bundling [31,36]. We also propose that formation of this higher-order structure may sterically occlude formation of tightly packed parallel bundles. As the CM mutants perturb the ability of MVt to inhibit bundling, we hypothesize that CM mutations within the insert impair formation of the protruding globular structure formed at the N-terminus.

To test this hypothesis, we assessed the effect of these mutants on the stability of the globule for each of the two clusters [40]. We find that A934V and R975W are indeed destabilizing to formation of the

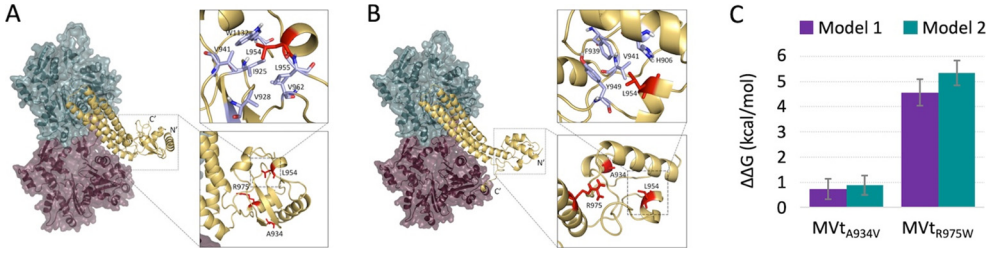

Fig. 6. Actin binding to MVt may induce a higher-order structural element that prevents F-actin bundling. DMD simulations identify two distinct MVt–actin clusters. In contrast to Vt, actin binding to MVt induces a protruding sub-domain. Representative MVt and F-actin models show that additional structure is formed between N-terminus, insert, and C-terminus in the first cluster (A) and between N-terminus and insert in the second cluster (B). MVt residues mutated in CMs (A934, L954, R975) are colored red. Point mutations A934V and R975W cause an increase in ΔΔG (D) and thus destabilize the folded sub-domain. These findings suggest that MVt CM mutants fail to antagonize Vt-induced actin bundling due to destabilization of the additional folded structure.

actin-induced MVt higher-order structure observed in both clusters. For the first model, ΔΔG-A934V = 0.73 ± 0.41 and ΔΔG-R975W = 4.56 ± 0.52, and for the second model, ΔΔG-A934V = 0.88 ± 0.39 and ΔΔG-R975W = 5.34 ± 0.49. We are unable to calculate ΔΔG for the ΔL954 since backbone is altered by the deletion [40]. However, we note that in each of the models, L954 forms an extensive network of hydrophobic contacts (zoomed in regions, Fig. 6A–B) and its deletion would be expected to cause disruptions of these networks. Interestingly, correlating with the severity of CM mutations [32,33], the R975W exhibits a much higher ΔΔG.

Discussion

Debilitating heart conditions resulting from CMs are a major health issue. According to the Centers for Disease Control and Prevention, as many as 1 in 500 adults may have this condition [41,42]. Both DCM and HCM have been shown to be associated with inherited and sporadic mutations in genes encoding the cardiac tissue-specific vinculin isoform, metavinculin. Here we have investigated the effects of disease-associated point mutations that occur within the 68-residue metavinculin insert that differentiates the actin-binding tail domains of vinculin (Vt) and metavinculin (MVt). We and others have previously shown that MVt lacks the actin bundling activity of Vt, and furthermore that MVt can negatively regulate the formation of Vt-induced bundles at physiologically relevant sub-stoichiometric ratios [26,27]. It is interesting to note that, while vinculin is ubiquitously expressed in all tissue types, metavinculin is co-expressed only in cardiac and smooth muscle cells. Both of these cell types exhibit a high degree of contractility for proper functioning, with increased metavinculin expression corresponding to the contractile load on the tissue [26]. Cardiomyocytes, in particular, undergo rapid contraction and expansion during beating for regular heart function. It is plausible that if only vinculin is present, the heart muscle would become stiff due to a large network of thick F-actin fibers and would not retain the necessary contractile properties. Co-expression of metavinculin may thus reduce vinculin-mediated actin bundling so that cardiac cells remain flexible and functional, acting as a molecular rheostat. The main finding of our study, that metavinculin CM mutants are dysfunctional in this regard, makes the strong prediction that cardiomyocytes expressing them should stiffen, and experiments are ongoing to test this hypothesis.

In this paper, we dissect the biophysical mechanisms underlying the metavinculin–vinculin interplay in F-actin fiber formation, and the dysregulation of this process by disease-associated point mutations in metavinculin. We previously reported that the N-terminal helices in both Vt (H1) and MVt (H1′) are released from the H2–H4 helical bundle upon actin engagement, and that Vt H1 residue M898, which is buried in the bundle's hydrophobic core in the pre-bound conformation, is important for actin bundling by Vt [31]. This led us to speculate that the H1 could mediate bundling contacts between Vt molecules after actin binding (Fig. 7A), and furthermore, that released H1′ and NtS′ plus upstream disordered sequence in MVt could be important for its inhibitory

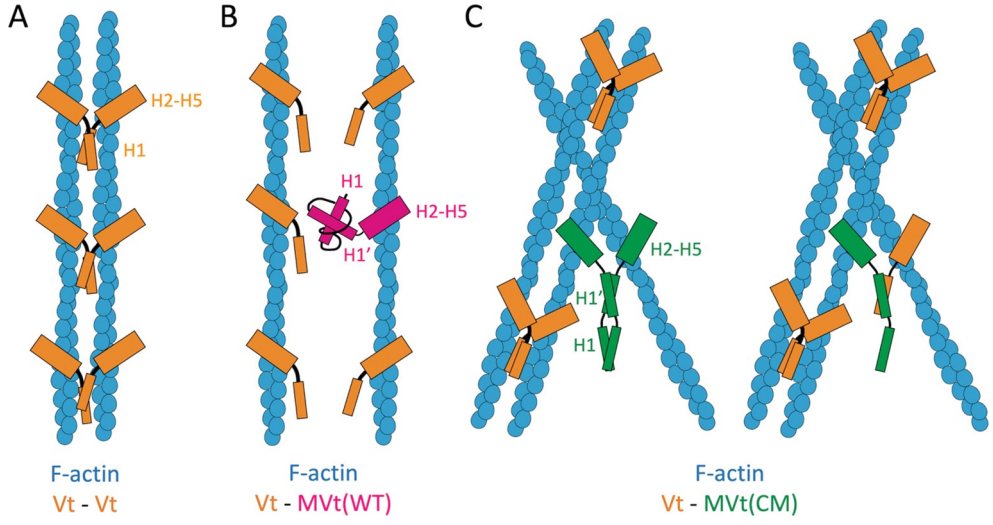

Fig. 7. Model for inhibition of Vt-induced F-actin bundle by WT MVt [labeled as MVt(WT)] but failure of that by MVt CM mutants [labeled as MVt(CM)]. (A) Release of H1 upon F-actin engagement enables Vt dimerization, thus resulting in parallel F-actin bundle formation. (B) An additional protruding structural sub-domain formed by the insert and displaced H1 at the N-terminus of MVt(WT) blocks homo- or hetero-dimer formation with Vt, thus preventing F-actin bundling. (C) The protruding sub-domain is destabilized by the CM related mutations in MVt(CM), resulting in disordered F-actin assemblies due to alternative interactions with another subunit of MVt(CM) (left) or a subunit of Vt (right).

activity by unknown mechanisms. As metavinculin CM-associated point mutants are located within the insert composing H1′ and NtS′, but distal from the direct actin-binding H2–H4 regions, we hypothesized that these lesions would compromise MVt's regulation of Vt-mediated actin bundling without impacting actin binding. The results we present here are broadly consistent with this model. Using co-sedimentation assays, we find that all of the CM mutants we examined have unimpaired actin binding affinity. However, both co-sedimentation assays and negative-stain EM experiments clearly demonstrate that all of the mutants have a strikingly similar defect in regulating Vt's actin bundling activity. These results strongly indicate that the H1′–NtS′ region is required for metavinculin's regulation of vinculin and furthermore motivate us to speculate that defects in this process may underlie the pathophysiology of metavinculin CM mutants *in vivo*, a hypothesis that will guide future cell biological and animal studies.

Mechanistically, our studies lead us to propose a steric occlusion model for metavinculin's ability to negatively regulate vinculin-mediated actin bundling in sub-stoichiometric amounts, orchestrated by differential folding of the MVt domain upon actin binding. Our simulation studies suggest that the MVt specific-insert coordinates the folding of a protruding globular sub-domain upon actin-binding-induced release from the H2–H4 helical bundle. While the detailed structure of the Vt-dimer that promotes 3D actin bundles is unknown and remains an important subject for future studies, electron tomographic studies of Vt-induced 2D F-actin arrays on lipid monolayers suggested that filaments are very tightly apposed when cross-linked by Vt, with intimate contacts between Vt molecules mediating the interface [43]. We thus propose that the MVt sub-domain acts a steric block and prevents actin filaments from coming close enough together for Vt molecules to bind (Fig. 7B). We note that this simple model readily explains the ability of sub-stoichiometric amounts of MVt to inhibit Vt bundling, as it does not require any specific molecular interactions between MVt and Vt to, for example, occupy a binding interface required for dimerization on Vt.

Consistent with this model, our computational studies suggest that MVt CM mutants destabilize sub-domain formation, thereby removing the steric block to Vt dimerization and bundle formation (a loss of function). Furthermore, the R975W substitution had the greatest impact on $\Delta\Delta G$ of sub-domain formation (Fig. 6C) consistent with the enhanced severity of this lesion *in vivo* [32,33] relative to the other the CM mutations we tested [32]. However, the sub-domain blockage model can only partially explain the behavior we observed for the CM mutants. All of the mutants we tested also have a gain-of-function effect on their own, inducing increased formation of higher-order F-actin assemblies (Fig. 3) with a disordered, mesh-like morphology. Furthermore, our studies suggest that the CM mutants drive the coalescence of Vt-induced bundles into aberrantly large assemblies (Fig. 5), which could also play a role in their pathophysiology *in vivo*. We speculate that CM mutations stimulate aggregation through the MVt insert region, which becomes exposed due to defects in sub-domain or globule folding, an effect that would be enhanced by high local concentrations within F-actin assemblies (Fig. 7C). Overall, our results suggest that small molecules that enhance the folding and stability of the predicted MVt globule may have therapeutic potential for patients with CM mutations in the metavinculin insert, abrogating both loss- and gain-of-function effects, and the findings we have presented will motivate future efforts in this direction.

While our studies have focused on Vt and MVt interactions with F-actin, vinculin is a scaffold protein that interacts with a number of proteins and inositol phospholipids (e.g., phosphatidylinositol 4,5-bisphosphate). Hence, the metavinculin insert may alter association with other ligands that bind to the tail domain. Experiments are in progress to investigate whether metavinculin coordinately regulates membrane association of vinculin through direct binding to phosphatidylinositol 4,5-bisphosphate or additional ligand interactions with the tail and proline-rich domain. Modulation of these additional interactions could affect localization, formation of structural assemblies, and mechanotransduction properties.

Materials and Methods

Protein expression and purification

Vt containing residues 879–1066 of the chicken sequence was cloned into pQlinkH vector (Addgene, Cambridge, MA). MVt containing residues 879–1134 and MVt plus proline-rich linker (MVtp) containing residues 858–1134 of the human sequence were cloned in 2HR-T vector (Addgene, Cambridge, MA). Plasmids for the MVt and MVtp CM mutants, namely, A934V, ΔL954, and R975W, were prepared using appropriate primers (IDT, Skokie, IL) and QuikChange site-directed mutagenesis kit (Stratagene, La Jolla, CA) and verified by DNA sequencing (Genewiz, South Plainfield, NJ). All of the Vt and MVt/MVtp vectors contained an N-terminal TEV cleavable hexa-histidine tag. Vectors were transformed into *Escherichia coli* strain BL21(DE3), and cells were first grown at 37 °C to an optical density of 0.6–0.8 (600 nm). Protein expression was then initiated by addition of IPTG (0.5 mM for Vt, 1 mM for MVt/MVtp). Cells were then grown at 18 °C overnight and harvested by centrifugation (4,500 rpm, 30 min). Cell pellets were resuspended in lysis

buffer [20 mM Tris, 150 mM NaCl, 5 mM imidazole, 2 mM β-mercaptoethanol (pH 7.5) for Vt and 50 mM Tris, 200 mM NaCl, 10 mM imidazole, 2 mM β-mercaptoethanol (pH 8.0) for MVt/MVtp]. Cells were lysed by sonication. Vt and MVt/MVtp proteins remained in the soluble fractions that were separated from the particulate fractions by centrifugation (15,000 rpm, 45 min). Proteins were purified by affinity separation using Ni-NTA-agarose beads (Qiagen). Proteins were bound to the beads through His-tag. Wash buffer [20 mM Tris, 150 mM NaCl, 60 mM imidazole, 2 mM β-mercaptoethanol (pH 7.5) for Vt and 50 mM Tris, 200 mM NaCl, 25 mM imidazole, 2 mM β-mercaptoethanol (pH 8.0) for MVt/MVtp) was run through the column before eluting target proteins using elution buffer [20 mM Tris, 150 mM NaCl, 500 mM imidazole, 2 mM β-mercaptoethanol (pH 7.5) for Vt and 50 mM Tris, 200 mM NaCl, 250 mM imidazole, 2 mM β-mercaptoethanol (pH 8.0) for MVt/MVtp). For His-tag removal, eluted volume was dialyzed into TEV cleavage buffer [20 mM Tris, 150 mM NaCl, 50 mM imidazole, 2 mM β-mercaptoethanol (pH 7.5) for Vt and 50 mM Tris, 200 mM NaCl, 20 mM imidazole, 2 mM β-mercaptoethanol (pH 8.0) for MVt/MVtp] overnight at 4 °C in presence of TEV protease. Vt and MVt/MVtp proteins were collected by re-running the dialyzed/cleaved volumes over Ni-NTA-agarose beads. Size exclusion chromatography by S100 column (GE, Pittsburg, PA) was used to obtain the highest level of purity in gel filtration buffer [10 mM Tris, 200 mM KCl, 10 mM imidazole, 2.5 mM $MgCl_2$, 1 mM EGTA, 2 mM DTT (pH 7.5)]. Purified proteins were concentrated between 200 and 500 μM by centrifugation, aliquoted, and snap frozen using liquid nitrogen. Protein stocks were stored at −80 °C.

Actin co-sedimentation

The actin binding and bundling (cross-linking) properties of individual Vt and MVt/MVtp WT and CM proteins as well as their mixtures were investigated using an adapted actin co-sedimentation assay previously reported [44]. Monomeric actin (G-actin), purified from rabbit muscle acetone powder (Pel-Freez Biologicals, Rogers, AR), was stored at −80 °C in storage buffer [50 mM imidazole, 100 mM NaCl, 10 mM $MgCl_2$, 10 mM EGTA, 0.5 mM DTT, 0.2 mM ATP (pH 7.0)]. Polymerization to filamentous actin (F-actin) was done by diluting and incubating G-actin at 100 μM concentration in actin polymerization buffer [10 mM Tris, 200 mM KCl, 10 mM imidazole, 2.5 mM $MgCl_2$, 1 mM EGTA, 2 mM DTT (pH 7.5)] at room temperature for 30 min. The actin concentrations reported in this work were based on G-actin concentration, since the heterogeneity of F-actin polymers made it difficult to quantify F-actin concentrations. Vt and MVt/MVtp variants were also diluted by actin polymerization buffer to prepare 100 μM stocks. To assess actin binding, 100 μl samples were prepared containing 10 μM Vt/MVt/MVtp variants and 10 or 20 μM actin. The samples were incubated at room temperature for 1 h and then centrifuged at 100,000 RCF for 30 min. To assess actin bundling, 100 μl samples were prepared containing 10–20 μM Vt/MVt/MVtp variants and 10 μM actin. The samples were incubated at room temperature for 1 h and then centrifuged at 12,000 RCF for 15 min. For both binding and bundling co-sedimentation, the supernatant and pellet were separated, resuspended to equal volumes, and analyzed by 15% SDS-PAGE. Actin binding properties were calculated by determining the fractions of Vt/MVt/MVtp variants present in pellets using the densities of the pellet and supernatant bands. Actin bundling properties were calculated by determining the fractions of actin present in pellets using the densities of the pellet and supernatant bands. Densitometry was performed using ImageJ [38]. Statistical significances (*p* values) of the measurements were determined using the Microsoft Excel t-Test function.

Negative staining and TEM

For the experiments displayed in Fig. 1, an aliquot of actin (1 μM) without or with Vt, MVt, or MVtp (10 μM) was incubated in actin polymerization buffer [10 mM Tris, 200 mM KCl, 10 mM imidazole, 2.5 mM $MgCl_2$, 1 mM EGTA, 2 mM DTT (pH 7.5)] for 15 min and absorbed directly onto glow-discharged carbon-coated 400 mesh copper grids for 3 min, and then stained with 2% (w/v) uranyl acetate in water. TEM images were obtained using a FEI Tecnai 12 electron microscope at 80 kV and captured on a Gatan First Light CCD camera using Gatan Digital Micrograph software (Gatan, Pleasanton, CA).

For the experiments displayed in Figs. 3 and 5, F-actin and the indicated Vt ± MVt constructs were mixed in KMEI [50 mM KCl, 1 mM $MgCl_2$, 1 mM ethylene glycol bis(*b*-aminoethyl ether) *N*,*N*′-tetraacetic acid (EGTA), 10 mM imidazole, 1 mM dithiothreitol (DTT), pH 7.0)] and incubated at room temperature for 15 min. Sample (4 μl) was then applied to a glow-discharged continuous carbon grid (Ted Pella) and incubated for 60 s. After incubation, the grid was washed with three 100 μl drops of 1% uranyl acetate, then blotted to dryness. Images were acquired with the SerialEM package [45] on a Tecnai F20 operating at 120 kV with a Gatan Ultrascan 4000 CCD camera. Tiled images with 20% overlap were acquired at 7800× magnification, 3 μm underfocus, and 4-fold camera binning, corresponding to a calibrated pixel size of 5.7 nm at the specimen level. Stitched images were assembled with the "blendmont" program from the IMOD software package [46].

F-actin assembly quantification

Images were thresholded and binarized using ImageJ [38], then segmented into continuous regions of pixels using the built-in "Analyze Particles" plugin, including regions 100–500,000 pixels in size and with a circularity of 0–0.3. This procedure does not always capture every region that an expert user would designate to contain F-actin in every image (e.g., areas of Supplementary Fig. 1A, right, which are not outlined in yellow). However, we find its performance superior to both manual segmentation of the images, which requires user decisions on region boundaries and the minimum size of regions, as well as a sliding-box quantification (a measure of local density), which is extremely sensitive to noise introduced by slight differences in thresholding (data not shown).

Size measurements of regions were pooled from all images for a given condition, then divided into 10,000 equal sized bins per data set and plotted via a normalized cumulative histogram (Supplementary Fig. 1B). Data were binned and cumulative sums calculated with a python script (available at www.github.com/alushinlab/FactinAssemblyQuant) using the function "binned_statistic" implemented in SciPy (www.scipy.org). Plots were generated and statistical tests were conducted with GraphPad Prism.

MD simulation

Modeling was performed using a DMD package [39,40,47]. The initial structure was obtained by extending missing N- and C-termini of MVt (PDB ID: 3JBK) [31] with PYMOL built-in tool to include residues 896–1134. The initial structure was relaxed at temperature $T = 0.5$ with high heat exchange coefficient $C_{ex} = 10$ for 10,000 steps. The temperature unit is kcal/(mol k_B).The relaxation was followed by replica exchange simulations with 10 replicas ($T = 0.330$, 0.360, 0.390, 0.420, 0.450, 0.480, 0.510, 0.540, 0.570, 0.600; $C_{ex} = 0.1$ for 2 million steps). Replicas were exchanged every 1000 steps. To preserve contacts between MVt and actin, we applied harmonic constraints to the N, CA, and C backbone atoms of selected residues (R1044, I1045, N1048, R1055, T1058, I1059, Q1062, I1065, Q1086, E1089, M1090, H1093, N1094, E1104, R1107, E1108, A1111, I1114). These constraints restrict atoms to move within 2A around initial positions. All atoms within actin were considered static and were not allowed to move. The 100 lowest-energy structures were selected and clustered based on pairwise root mean square distance between structures. Two clusters were identified.

Structures representing the centroids of the two clusters were subject to DMD simulations at two constant temperatures $T_1 = 0.5$ kcal/(mol k_B) and $T_2 = 0.55$ kcal/(mol k_B). For each temperature and for each structure, 5 independent simulations were run for 1 million steps with $C_{ex} = 0.1$. To preserve contacts between MVt and actin, we applied harmonic constraints to N, CA, and C backbone atoms of selected MVt residues (as described above). All atoms within actin were considered static.

Acknowledgments

We gratefully acknowledge Jenny Hinshaw (NIDDK) for shared use of her F20 TEM and Lucas Axiotakis Jr. for preliminary efforts in quantification of EM data. This work was supported by the National Institutes of Health (RO1GM115597, PI: S.C.; 7DP5OD017885, PI: G.M.A.; (F31HL131429, PI: H. L.; GM31819 and ES013773, PI: J.G.; GM114015 and GM123247, PI: N. V. D.) and start-up funds from the Rockefeller University (PI: G.M.A).

Appendix A. Supplementary data

Supplementary data to this article can be found online at https://doi.org/10.1016/j.jmb.2019.02.024.

Received 27 November 2018;
Received in revised form 22 February 2019;
Accepted 22 February 2019
Available online 5 March 2019

Keywords:
vinculin;
metavinculin;
actin;
cardiomyopathy;
heart

Present address: Departments of Pharmacology, Biochemistry & Molecular Biology, Pennsylvania State College of Medicine, Hershey, PA 17033, USA.

Abbreviations used:
Vh, vinculin head domain; Vt, vinculin tail domain; MVt, metavinculin tail domain; CM, cardiomyopathy; NtS, N-terminal strap; CtHP, C-terminal hairpin; DCM, dilated cardiomyopathy; HCM, hypertrophic cardiomyopathy; WT, wild-type; DMD, discrete molecular dynamics; TEM, transmission electron microscopy.

References

[1] J.T. Parsons, A.R. Horwitz, M.A. Schwartz, Cell adhesion: integrating cytoskeletal dynamics and cellular tension, Nat. Rev. Mol. Cell Biol. 11 (2010) 633–643.
[2] W.H. Ziegler, R.C. Liddington, D.R. Critchley, The structure and regulation of vinculin, Trends Cell Biol. 16 (2006) 453–460.

[3] W. Xu, H. Baribault, E.D. Adamson, Vinculin knockout results in heart and brain defects during embryonic development, Development 125 (1998) 327–337.
[4] J.L. Coll, A. Ben-Ze'ev, R.M. Ezzell, J.L. Rodriguez Fernandez, H. Baribault, R.G. Oshima, E.D. Adamson, Targeted disruption of vinculin genes in F9 and embryonic stem cells changes cell morphology, adhesion, and locomotion, Proc. Natl. Acad. Sci. U. S. A. 92 (1995) 9161–9165.
[5] M.C. Subauste, O. Pertz, E.D. Adamson, C.E. Turner, S. Junger, K.M. Hahn, Vinculin modulation of paxillin–FAK interactions regulates ERK to control survival and motility, J. Cell Biol. 165 (2004) 371–381.
[6] C. Bakolitsa, D.M. Cohen, L.A. Bankston, A.A. Bobkov, G.W. Cadwell, L. Jennings, D.R. Critchley, S.W. Craig, R.C. Liddington, Structural basis for vinculin activation at sites of cell adhesion, Nature 430 (2004) 583–586.
[7] R.P. Johnson, S.W. Craig, An intramolecular association between the head and tail domains of vinculin modulates talin binding, J. Biol. Chem. 269 (1994) 12611–12619.
[8] E.E. Weiss, M. Kroemker, A.H. Rudiger, B.M. Jockusch, M. Rudiger, Vinculin is part of the cadherin–catenin junctional complex: complex formation between alpha-catenin and vinculin, J. Cell Biol. 141 (1998) 755–764.
[9] M. Kroemker, A.H. Rudiger, B.M. Jockusch, M. Rudiger, Intramolecular interactions in vinculin control alpha-actinin binding to the vinculin head, FEBS Lett. 355 (1994) 259–262.
[10] N.P. Brindle, M.R. Holt, J.E. Davies, C.J. Price, D.R. Critchley, The focal-adhesion vasodilator-stimulated phosphoprotein (VASP) binds to the proline-rich domain in vinculin, Biochem J 318 (1996) 753–757 Pt 3.
[11] K.A. DeMali, C.A. Barlow, K. Burridge, Recruitment of the Arp2/3 complex to vinculin: coupling membrane protrusion to matrix adhesion, J. Cell Biol. 159 (2002) 881–891.
[12] N. Kioka, S. Sakata, T. Kawauchi, T. Amachi, S.K. Akiyama, K. Okazaki, C. Yaen, K.M. Yamada, S. Aota, Vinexin: a novel vinculin-binding protein with multiple SH3 domains enhances actin cytoskeletal organization, J. Cell Biol. 144 (1999) 59–69.
[13] K. Mandai, H. Nakanishi, A. Satoh, K. Takahashi, K. Satoh, H. Nishioka, A. Mizoguchi, Y. Takai, Ponsin/SH3P12: an l-afadin- and vinculin-binding protein localized at cell–cell and cell–matrix adherens junctions, J. Cell Biol. 144 (1999) 1001–1017.
[14] S. Huttelmaier, P. Bubeck, M. Rudiger, B.M. Jockusch, Characterization of two F-actin-binding and oligomerization sites in the cell-contact protein vinculin, Eur. J. Biochem. 247 (1997) 1136–1142.
[15] R.P. Johnson, V. Niggli, P. Durrer, S.W. Craig, A conserved motif in the tail domain of vinculin mediates association with and insertion into acidic phospholipid bilayers, Biochemistry 37 (1998) 10211–10222.
[16] J.H. Lee, E.S. Rangarajan, S.D. Yogesha, T. Izard, Raver1 interactions with vinculin and RNA suggest a feed-forward pathway in directing mRNA to focal adhesions, Structure 17 (2009) 833–842.
[17] J. Winkler, H. Lunsdorf, B.M. Jockusch, The ultrastructure of chicken gizzard vinculin as visualized by high-resolution electron microscopy, J. Struct. Biol. 116 (1996) 270–277.
[18] J. Golji, T. Wendorff, M.R. Mofrad, Phosphorylation primes vinculin for activation, Biophys. J. 102 (2012) 2022–2030.
[19] C.G. Galbraith, K.M. Yamada, M.P. Sheetz, The relationship between force and focal complex development, J. Cell Biol. 159 (2002) 695–705.
[20] G. Giannone, G. Jiang, D.H. Sutton, D.R. Critchley, M.P. Sheetz, Talin1 is critical for force-dependent reinforcement of initial integrin-cytoskeleton bonds but not tyrosine kinase activation, J. Cell Biol. 163 (2003) 409–419.
[21] D. Riveline, E. Zamir, N.Q. Balaban, U.S. Schwarz, T. Ishizaki, S. Narumiya, Z. Kam, B. Geiger, A.D. Bershadsky, Focal contacts as mechanosensors: externally applied local mechanical force induces growth of focal contacts by an mDia1-dependent and ROCK-independent mechanism, J. Cell Biol. 153 (2001) 1175–1186.
[22] C. Grashoff, B.D. Hoffman, M.D. Brenner, R. Zhou, M. Parsons, M.T. Yang, M.A. McLean, S.G. Sligar, C.S. Chen, T. Ha, M.A. Schwartz, Measuring mechanical tension across vinculin reveals regulation of focal adhesion dynamics, Nature 466 (2010) 263–266.
[23] B.J. Byrne, Y.J. Kaczorowski, M.D. Coutu, S.W. Craig, Chicken vinculin and meta-vinculin are derived from a single gene by alternative splicing of a 207-base pair exon unique to meta-vinculin, J. Biol. Chem. 267 (1992) 12845–12850.
[24] K. Burridge, J.R. Feramisco, Microinjection and localization of a 130K protein in living fibroblasts: a relationship to actin and fibronectin, Cell 19 (1980) 587–595.
[25] J.R. Feramisco, J.E. Smart, K. Burridge, D.M. Helfman, G.P. Thomas, Co-existence of vinculin and a vinculin-like protein of higher molecular weight in smooth muscle, J. Biol. Chem. 257 (1982) 11024–11031.
[26] A.M. Belkin, O.I. Ornatsky, A.E. Kabakov, M.A. Glukhova, V. E. Koteliansky, Diversity of vinculin/meta-vinculin in human tissues and cultivated cells. Expression of muscle specific variants of vinculin in human aorta smooth muscle cells, J. Biol. Chem. 263 (1988) 6631–6635.
[27] S. Witt, A. Zieseniss, U. Fock, B.M. Jockusch, S. Illenberger, Comparative biochemical analysis suggests that vinculin and metavinculin cooperate in muscular adhesion sites, J. Biol. Chem. 279 (2004) 31533–31543.
[28] M. Maeda, E. Holder, B. Lowes, S. Valent, R.D. Bies, Dilated cardiomyopathy associated with deficiency of the cytoskeletal protein metavinculin, Circulation 95 (1997) 17–20.
[29] E.S. Rangarajan, J.H. Lee, S.D. Yogesha, T. Izard, A helix replacement mechanism directs metavinculin functions, PLoS One 5 (2010), e10679.
[30] M.E. Janssen, H. Liu, N. Volkmann, D. Hanein, The C-terminal tail domain of metavinculin, vinculin's splice variant, severs actin filaments, J. Cell Biol. 197 (2012) 585–593.
[31] L.Y. Kim, P.M. Thompson, H.T. Lee, M. Pershad, S.L. Campbell, G.M. Alushin, The structural basis of actin organization by vinculin and metavinculin, J. Mol. Biol. 428 (2016) 10–25.
[32] T.M. Olson, S. Illenberger, N.Y. Kishimoto, S. Huttelmaier, M. T. Keating, B.M. Jockusch, Metavinculin mutations alter actin interaction in dilated cardiomyopathy, Circulation 105 (2002) 431–437.
[33] V.C. Vasile, M.L. Will, S.R. Ommen, W.D. Edwards, T.M. Olson, M.J. Ackerman, Identification of a metavinculin missense mutation, R975W, associated with both hypertrophic and dilated cardiomyopathy, Mol. Genet. Metab. 87 (2006) 169–174.
[34] K. Shen, C.E. Tolbert, C. Guilluy, V.S. Swaminathan, M.E. Berginski, K. Burridge, R. Superfine, S.L. Campbell, The vinculin C-terminal hairpin mediates F-actin bundle formation, focal adhesion, and cell mechanical properties, J. Biol. Chem. 286 (2011) 45103–45115.
[35] R.P. Johnson, S.W. Craig, Actin activates a cryptic dimerization potential of the vinculin tail domain, J. Biol. Chem. 275 (2000) 95–105.

[36] Z.A. Oztug Durer, R.M. McGillivary, H. Kang, W.A. Elam, C.L. Vizcarra, D. Hanein, E.M. De La Cruz, E. Reisler, M.E. Quinlan, Metavinculin tunes the flexibility and the architecture of vinculin-induced bundles of actin filaments, J. Mol. Biol. 427 (2015) 2782–2798.
[37] T. Meyer, U. Brink, C. Unterberg, S. Stohr, H. Kreuzer, A.B. Buchwald, Expression of meta-vinculin in human coronary arteriosclerosis is related to the histological grade of plaque formation, Atherosclerosis 111 (1994) 111–119.
[38] C.A. Schneider, W.S. Rasband, K.W. Eliceiri, NIH image to ImageJ: 25 years of image analysis, Nat. Methods 9 (2012) 671–675.
[39] F. Ding, D. Tsao, H. Nie, N.V. Dokholyan, Ab initio folding of proteins with all-atom discrete molecular dynamics, Structure 16 (2008) 1010–1018.
[40] S. Yin, F. Ding, N.V. Dokholyan, Eris: an automated estimator of protein stability, Nat. Methods 4 (2007) 466–467.
[41] B.J. Maron, J.J. Doerer, T.S. Haas, D.M. Tierney, F.O. Mueller, Sudden deaths in young competitive athletes: analysis of 1866 deaths in the United States, 1980–2006, Circulation 119 (2009) 1085–1092.
[42] B.J. Maron, W.J. McKenna, G.K. Danielson, L.J. Kappenberger, H.J. Kuhn, C.E. Seidman, P.M. Shah, W.H. Spencer 3rd, P. Spirito, F.J. Ten Cate, E.D. Wigle, American College of Cardiology/European Society of Cardiology clinical expert consensus document on hypertrophic cardiomyopathy. A report of the American College of Cardiology Foundation Task Force on Clinical Expert Consensus Documents and the European Society of Cardiology Committee for Practice Guidelines, J. Am. Coll. Cardiol. 42 (2003) 1687–1713.
[43] M.E. Janssen, E. Kim, H. Liu, L.M. Fujimoto, A. Bobkov, N. Volkmann, D. Hanein, Three-dimensional structure of vinculin bound to actin filaments, Mol. Cell 21 (2006) 271–281.
[44] R.D. Dixon, D.K. Arneman, A.S. Rachlin, N.R. Sundaresan, M.J. Costello, S.L. Campbell, C.A. Otey, Palladin is an actin cross-linking protein that uses immunoglobulin-like domains to bind filamentous actin, J. Biol. Chem. 283 (2008) 6222–6231.
[45] D.N. Mastronarde, Automated electron microscope tomography using robust prediction of specimen movements, J. Struct. Biol. 152 (2005) 36–51.
[46] J.R. Kremer, D.N. Mastronarde, J.R. McIntosh, Computer visualization of three-dimensional image data using IMOD, J. Struct. Biol. 116 (1996) 71–76.
[47] E.A. Proctor, F. Ding, N.V. Dokholyan, Discrete molecular dynamics, Wiley I.R.C. Mol. Sci. 1 (2011) 80–92.